Modern Physics Letters B
(2023) 2350233 (17 pages)

DOI: 10.1142/S0217984923502330

Broadband supercontinuum generation in hollow-core photonic crystal fibers infiltrated with chloroform

Thuy Nguyen Thi*,‡ and Lanh Chu Van†,§

*University of Education, Hue University,
34 Le Loi, Hue City, Viet Nam

†Department of Physics, Vinh University,
182 Le Duan, Vinh City, Viet Nam
‡ntthuy@hueuni.edu.vn; nguyenthithuy@dhsphue.edu.vn
§chuvanlanh@vinhuni.edu.vn

Received 7 March 2023
Revised 11 May 2023
Accepted 24 June 2023
Published 23 August 2023

The chloroform-infiltrated square lattice photonic crystal fibers (PCFs) are designed with the difference of the air hole diameters in the cladding to improve chromatic dispersion and nonlinear properties. Based on numerical simulation results, two optimal structures with flat dispersion, high nonlinear coefficient, and small confinement loss are used for supercontinuum (SC) generation. The first fiber has an all-normal dispersion regime, a nonlinear coefficient of 486.355 $W^{-1}.km^{-1}$ generating an SC spectrum of 640.3 nm within 30 dB levels at a pump wavelength of 0.945 μm with peak power as low as 1.44 kW. With anomalous dispersion properties, the second fiber gives a very broad SC spectrum of 1471.8 nm within 30 dB levels at a 1.4 μm pumping wavelength with a peak power of 20 kW. All-fiber SC sources operating with low-power pump lasers can use these fibers to effectively replace glass-core fibers.

Keywords: PCF; $CHCl_3$ infiltration; broadband supercontinuum generation; low peak power; all-normal dispersion; anomalous dispersion.

1. Introduction

In recent years, different approaches to photonic crystal fibers (PCFs) in numerical simulation as well as in experiment have been implemented to obtain high supercontinuum (SC) generation efficiency and enhance its applicability in practice. Many new nonlinear materials have been developed, diversifying the non-silica-based fiber technology.[1–8] However, silica-based PCFs have always been attractive to research groups because they are a traditional optical fiber material, suitable for practical fiber fabrication despite limitations in extending the SC spectrum. Furthermore, the

‡Corresponding author.

advancement of fiber fabrication technology has made it possible to fabricate silica fibers with many new designs. Therefore, every attempt to enhance the nonlinear performance of silica fibers[9–12] and widen the scope of SC applications has been verified in many publications.[12–17] One of the ways of interest is to fill the hollow core of the PCF with a highly nonlinear liquid. The advantages offered by these PCFs include controllable dispersion properties, improved nonlinear properties, broad spectrum SC generation, and experimentally fabricable fibers. The diverse dispersion properties including all-normal (ANDi) and anomalous dispersion regimes are obtained in the PCFs.[18–20] Flat dispersion, small value, even ultra-flat, and near-zero in a wide wavelength range has been found in some recent studies.[21,22] Moreover, the nonlinearity of PCF is significantly improved i.e. one achieves a high nonlinear coefficient, small effective mode region, and low confinement loss, which can be beneficial for the SC process.[23–25] Unlike silica, nonlinear fluids show high nonlinearity and hence can generate a broad SC spectrum in a very short length of optical fiber with relatively lower input power.[26,27] In the experiment, highly nonlinear liquids were filled into the cores of PCFs by integrating a microfluidic pumping system using a thermal fusion splicer or laser writing technique.[28] These fibers can be easily fabricated by the conventional stack-and-draw method.[20]

The way in which nonlinear effects occur to govern the SC spectrum expansion and generate new frequency components as the laser pulse propagates in a highly nonlinear liquid-infiltrated PCF is strongly dependent on its dispersion profile. When the input pulse is excited in the normal dispersion mode, the soliton dynamics and related nonlinear effects can be avoided, but the spectral bandwidth is not significantly broadened. ANDi PCF with a convex dispersion regime, flattened near the pump wavelength, can produce a highly coherent, flat-top SC spectrum due to the dominance of self-phase modulation (SPM) effect, followed by optical wave breaking (OWB) but pump wavelength is higher than that of conventional.[20,25,29] The soliton dynamics[30] including soliton fission (SF), soliton self-frequency shift (SSFS), and blue-shifted dispersive waves (DWs) are responsible for the SC spectrum expansion when the input pulse is excited in the anomalous dispersion regime. The spectral bandwidth is significantly broadened with lower pump power but the spectrum is noisy.[19,27]

So far, there have been only a few publications on the generation of SC using silica-based PCFs filled with hollow-core by chloroform ($CHCl_3$). The high nonlinearity of these fibers implies that SC with broadband can be generated with low peak power pump pulses in a short-length fiber. SC spectrum expansion to 1100 nm with a peak power of 2 kW and within a short propagating distance of only 5 mm was observed in $CHCl_3$-infiltrated PCFs into the air core.[31] The highly coherent spectrum, with a bandwidth of 1020 nm, is testified in $CHCl_3$-filled PCF with appropriate geometric parameters. Although the nonlinear coefficient of the PCF is quite small, 640 $W^{-1} \cdot km^{-1}$, it still allows the propagation of the laser pulse in the 1 cm-long fiber with a peak power of 47 kW.[32] Meanwhile, the work[33] shows that the SC spectrum can be achieved with broadband 660 nm and 800 nm within two fibers with an

all-normal and anomalous dispersion regime with 2.5 kW peak power. The nonlinear coefficients of the fibers are $1290\,\mathrm{W}^{-1}\cdot\mathrm{km}^{-1}$ and $440\,\mathrm{W}^{-1}\cdot\mathrm{km}^{-1}$, respectively.

$CHCl_3$ can become a typical choice for use in highly nonlinear liquid-core PCFs due to some of its interesting characteristics. Although the nonlinearity of $CHCl_3$ ($n_2 = 1.64\times10^{-19}\,\mathrm{m}^2\cdot\mathrm{W}^{-1}$)[34] is lower than that of toluene (C_7H_8) ($n_2 = 16\times10^{-19}\,\mathrm{m}^2\cdot\mathrm{W}^{-1}$) and carbon disulfide ($CS_2$) ($n_2 = (4.3-5.1)\times10^{-18}\ \mathrm{m}^2\cdot\mathrm{W}^{-1}$), which might be equivalent to carbon tetrachloride (CCl_4) ($1.53\times10^{-19}\,\mathrm{m}^2\cdot\mathrm{W}^{-1}$) but it is one order of magnitude higher than fused silica (SiO_2) ($n_2 = 2.74\times10^{-20}\,\mathrm{m}^2\cdot\mathrm{W}^{-1}$).[35] This allows the electromagnetic field modes to be better confined in the core of the PCF. In practical applications, the toxicity of liquids infiltrating PCF is a safety concern. The advantage of $CHCl_3$ is its negligible toxicity when compared with CS_2 and C_7H_8.[36] To design single-mode silica PCFs efficiently, coupling with the standard silica fibers used in the all-fiber pump laser system is extremely important. Fortunately, the linear refractive index of $CHCl_3$ is only about 0.012 lower than that of silica. This enables the fabrication of $CHCl_3$-infiltrated silica fibers in practice to achieve higher coupling efficiency.[37]

Some research results on SC generation through hollow-core PCF filled with other liquids such as tetrachlorethylene (C_2Cl_4), ethanol (C_2H_5OH), benzene (C_6H_6) and nitrobenzene ($C_6H_5NO_2$) are presented in Table 1.

In the experiment, square-lattice PCF can be performed with a standard fabrication process, stack, and draw. It is also useful in the integrated optical devices

Table 1. Overview of SC generation in several liquids-infiltrated PCFs.

Structures	Liquids	Fiber length (cm)	Pump wavelength (μm)	Dispersion regime	SC range (nm)	Input peak power (kW)	Refs.
Hexagonal ($\#F_1$)	C_2Cl_4	5	1.56	all-normal	1180	16.67	18
Hexagonal ($\#F_2$)		10	1.56	anomalous	1000	16.67	
Hexagonal ($\#F_3$)		10	1.03	anomalous	1700	20.83	
Hexagonal ($\#F_1$)	CCl_4	30	1.35	anomalous	1300	2.67	20
Hexagonal ($\#F_2$)		30	1.064	all-normal	350	2.67	
Hexagonal	C_2H_5OH	20	1.55	anomalous	1000	50	22
Circular ($\#F_1$)	C_7H_8	1	1.064	all-normal	800	0.45	23
Circular ($\#F_2$)		10	1.55	anomalous	1100	0.56	
Hexagonal ($\#F_1$)	C_6H_6	1	1.55	all-normal	1300	55	25
Hexagonal ($\#F_2$)		1	1.55	anomalous	2000	37	
Hexagonal ($\#F_3$)		1	1.55	anomalous	2900	37	
Hexagonal ($\#L0.3$)	C_7H_8	10	1.55	all-normal	575	7.14	27
Hexagonal ($\#L0.35$)		10	1.55	anomalous	750	6.67	
Hexagonal ($\#F_1$)	$C_6H_5NO_2$	5	1.03	anomalous	1000	0.83	29
Hexagonal ($\#F_2$)		5	1.56	all-normal	1300	5.56	
Hexagonal ($\#F_3$)		5	1.56	anomalous	1000	0.67	
Hexagonal	$CHCl_3$	0.5	0.8	anomalous	850	2	31
Hexagonal	$CHCl_3$	1	1.06	anomalous	1020	47	32
Hexagonal ($\#F_1$)	$CHCl_3$	10	0.92	all-normal	660	2.5	33
Hexagonal ($\#F_2$)		10	1.03	anomalous	800	2.5	
Hexagonal	CS_2	14	1.56	anomalous	640	560	38

of a rectangular or a square cross-section with pig-tail fibers.[39] Some publications show that high birefringence, dispersion compensation, low confinement, and large mode area for data transmission can be achieved by introducing defects into square-lattice PCFs.[40] It can be seen that square-lattice PCF has not yet been extensively investigated in fiber fabrication experiments and other promising applications of SC generation. The results of our study illustrate the potential of the selected optimal structures for applications involving low peak power and broadband SC. In this report, we investigate $CHCl_3$-infiltrating PCF-based SC with a square lattice for the first time. The fibers' chromatic dispersion and nonlinear properties are investigated in detail based on numerical simulation results. The ability to generate a broad SC spectrum with low peak power is also verified for two optimal fibers. With a nonlinear coefficient as high as $486.355\,\mathrm{W}^{-1}\cdot\mathrm{km}^{-1}$, the first fiber emits a broad SC spectrum of 640.3 nm within 30 dB levels in an all-normal dispersion regime with a low peak power of 1.44 kW. The cause of the spectral expansion is attributed to the SPM effect. The soliton dynamics enable the SC spectrum to be broadened to 1471.8 nm at 30 dB levels with a peak power of 20 kW using a second fiber with an anomalous dispersion regime. Although this fiber has a nonlinear coefficient about nine times smaller than the first fiber, the low dispersion of -1.631 ps/nm.km at the pump wavelength is an advantage for the SC spectrum expansion.

2. Numerical Modeling of the PCFs

At the center of the PCF is a hollow core filled with $CHCl_3$, eight regularly arranged layers of air holes surrounding the core in a square lattice. Defects are reasonably introduced to optimize the dispersion and nonlinear properties of the fiber. The geometric cross-sections of the PCFs are described in Fig. 1(a). The work[41] demonstrated the effect of dispersion improvement, including zero-dispersion wavelength (ZDW) shift when modifying the size of the innermost layer. The attenuation of the fundamental mode and even the higher modes is also affected by the size of the remaining layers. Inspired by this, we designed PCFs with a filling factor d_1/Λ varying from 0.3 to 0.8 with a step of 0.5 (d_1 being the diameter of the air holes of the first layer near the core) while d_2/Λ is kept 0.95 constant (d_2 is the diameter of the other layer's air holes). The distance from the center of the core to the air holes and between the air holes is called lattice pitch Λ, Λ changes by 1.0, 1.5, 1.8, and 2.0 μm. The core diameter of the PCF is also an essential structural parameter because the size of the core affects its ability to be confined in light modes. It is always important to keep the core size as consistent as possible because it is small enough to enable dispersion engineering by designing photonic cladding and large enough to reasonably match the PCF-mode field diameters with the telecommunication single mode fiber. Our PCFs with core diameters determined by the formula $D_c = 2\Lambda - 1.1d_1$ ensure an effective guide index with reasonably large-mode field diameters. This improves dispersion to match conventional femtosecond laser pumps. The electromagnetic field modes are well confined in the PCF core, as shown in Fig. 1(b).

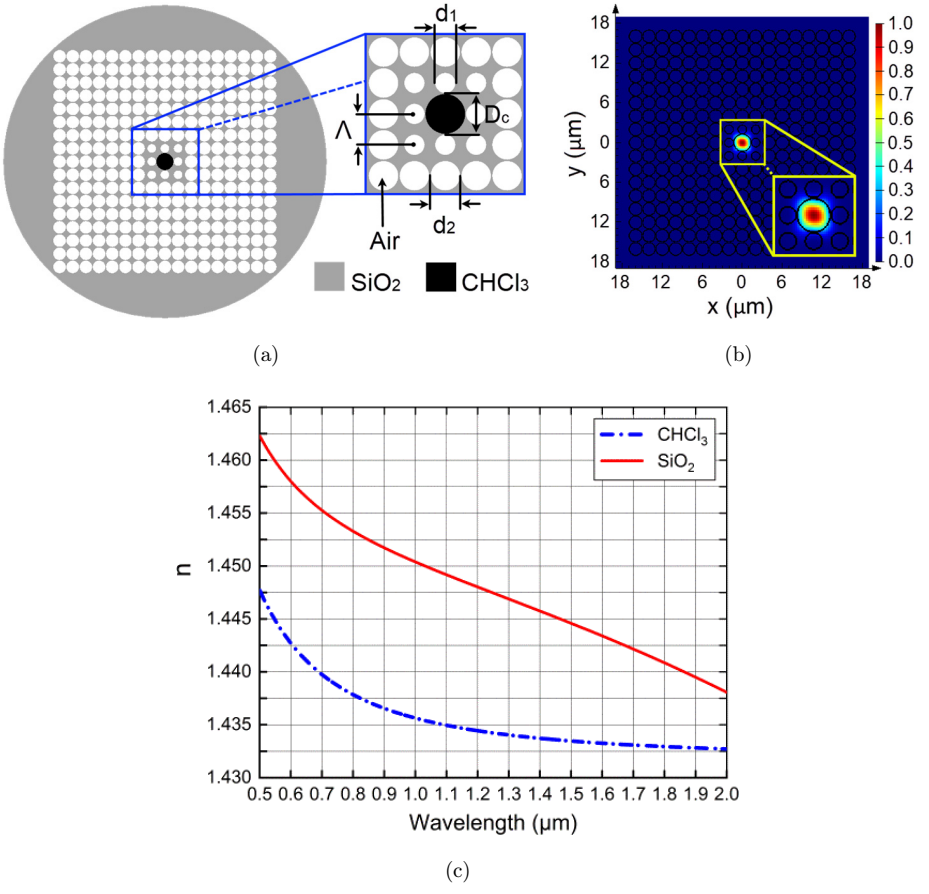

Fig. 1. (Color online) (a) Cross-section view of the circular $CHCl_3$-PCF; (b) the light confinement in the core of PCF with $\Lambda = 2.0\,\mu$m, $d_1/\Lambda = 0.65$, and (c) the real parts of the refractive index n of $CHCl_3$ and SiO_2.

Figure 1(c) illustrates the real parts of the refractive index n of chloroform and fused silica versus wavelength. By declaring the coefficients in the Sellmeier equations describing the wavelength-dependent refractive index characteristics of SiO_2[42] and $CHCl_3$[33] (Eqs. (1) and (2)) in the data system of the LMS software, along with the selection of appropriate structural parameters, we have successfully designed the PCF. Furthermore, the full-vector finite-difference eigenmode (FDE) method helps to analyze the propagation characteristics of light pulses in PCF by solving Maxwell's wave equations. Boundary conditions are perfectly matched layers that minimize reflection at the boundary and reduce loss. In our simulation, the cross-section of the fiber is divided into small rectangular sections called "Yee's mesh" to calculate the propagation constants β with high accuracy using a "FDE solver".[43] The optical properties in each Yee's mesh are approximated as unchanged. An index averaging technique is used for the cells across interfaces at points lying on

the surface between two media. The minimum mesh step of 10-6 μm and 300 mesh cells without override regions is set for PCFs. Significant losses of $CHCl_3$ were also assumed when performing these simulations. The wavelength region selected for investigation is 0.6–2.0 μm which is compatible with the reliable data in the LMS.

$$n^2_{SiO_2}(\lambda) = 1 + \frac{0.6961663\lambda^2}{\lambda^2 - (0.0684043)^2} + \frac{0.4079426\lambda^2}{\lambda^2 - (0.1162414)^2} + \frac{0.8974794\lambda^2}{\lambda^2 - (9.896161)^2}, \quad (1)$$

$$n^2_{CHCl_3}(\lambda) = 1 + \frac{1.04647\lambda^2}{\lambda^2 - 0.01048} + \frac{0.00345\lambda^2}{\lambda^2 - 0.15207}, \quad (2)$$

where λ is the excitation wavelength in micrometers, $n(\lambda)$ is the wavelength-dependent linear refractive index of materials.

$CHCl_3$ has transparency over a wide wavelength range, the relationship between attenuation A and wavelength is described in Eq. (3).[33] The absorption peaks of $CHCl_3$ are at wavelengths 1.152, 1.410, and 1.691 μm, respectively.[44] In addition, another stronger absorption peak close to 2380 nm is also observed.[45] The absorption peak at 1.691 μm corresponding to A at this wavelength is equal to 85.6 dB/cm. Therefore, we also assume that the fiber loss is 85.6 dB/cm over the wavelength range greater than 1.691 μm. These strong absorption peaks will probably create a gap in the SC spectrum when the fiber loss is approximately 85.6 dB/cm.[45]

$$A = 10\log[e^{(4\pi k/\lambda)}]. \quad (3)$$

3. Optical Properties of the PCFs

When the input pulse is short enough ($\leq$ 10 ps), the higher-order modes have a negligible effect on the SC broadening,[46] so we analyze only the fundamental mode dispersion. The material dispersion and waveguide dispersion are characterized by chromatic dispersion (D) and are determined by the following formula[47]:

$$D = -\frac{\lambda}{c}\frac{\partial^2 \mathrm{Re}[n_{\mathrm{eff}}]}{\partial\lambda^2}, \quad (4)$$

where λ and c are the wavelength and the speed of light in a vacuum, respectively, and $\mathrm{Re}[n_{\mathrm{eff}}]$ is the real part of the effective index of the guided mode.

The nonlinear coefficient is inversely proportional to the effective mode area[48] and the confinement loss[49] refers to the nonlinear characteristics that govern the SC efficiency. They are determined by the following formulas:

$$\gamma(\lambda) = 2\pi\frac{n_2}{\lambda A_{\mathrm{eff}}}, \quad (5)$$

with n_2 as the nonlinear refractive index for fused silica.

$$A_{eff} = \frac{\left(\int_{-\infty}^{\infty}\int_{-\infty}^{\infty}|E|^2 dxdy\right)^2}{\int_{-\infty}^{\infty}\int_{-\infty}^{\infty}|E|^4 dxdy}, \quad (6)$$

where E is the amplitude of the transverse electric field propagating inside the PCF.

$$L_c = 8.686 \frac{2\pi}{\lambda} \mathrm{Im}[n_{\mathrm{eff}}(\lambda)]. \tag{7}$$

The resulting graph of numerical simulation of wavelength-dependent dispersion curves is consistent with Eq. (4). Furthermore, the dispersion properties of the PCFs are also strongly influenced by the variation of the filling factor d_1/Λ and the lattice constants Λ which are observed for these $CHCl_3$-infiltrated PCFs. Equation (4) also shows the relationship between the dispersion coefficient D and the effective refractive index of the PCFs. Therefore, when the d_1/Λ and Λ vary, the effective refractive index between the core and the shell of the PCF will change, causing the dispersion properties to change as well. All-normal and anomalous dispersion properties are observed for PCFs with small lattice pitch Λ ($\Lambda = 1.0\,\mu$m) (Fig. 2(a)). Anomalous dispersions with one ZDW and two ZDWs are found when $d_1/\Lambda \leq 0.5$ and $d_1/\Lambda \geq 0.6$. In this case, only an all-normal dispersion is obtained with

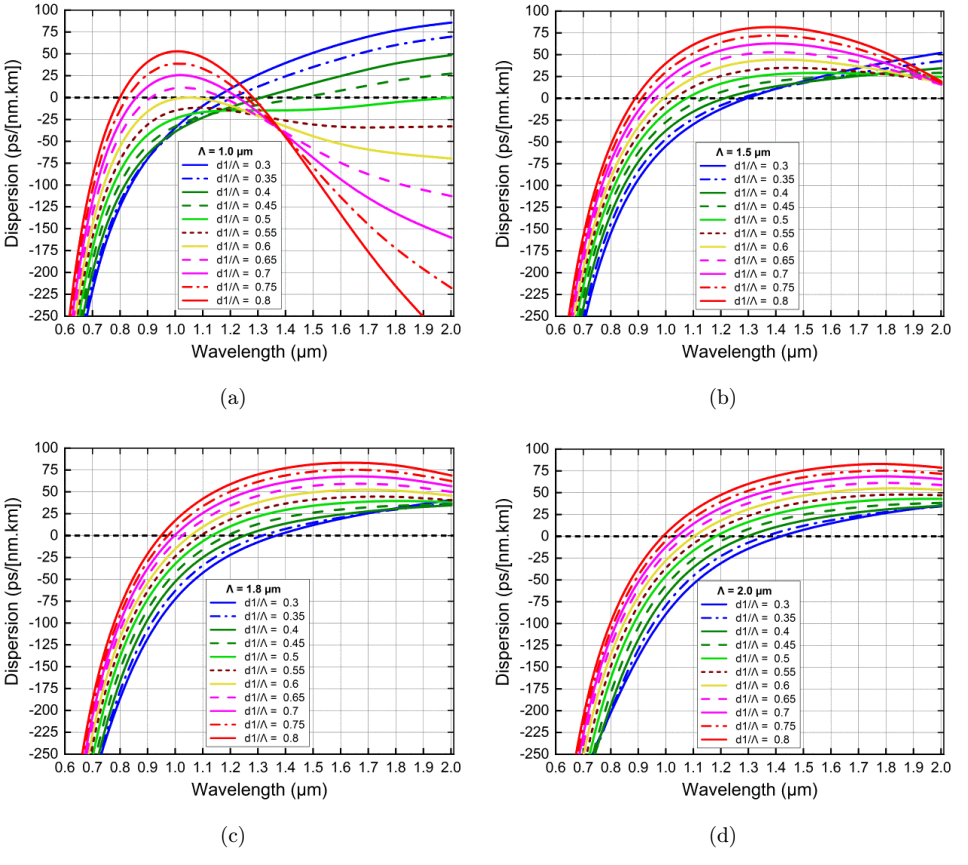

Fig. 2. (Color online) The chromatic dispersion characteristics of $CHCl_3$-PCFs with various values of d_1/Λ and (a) $\Lambda = 1.0\,\mu$m, (b) $1.5\,\mu$m, (c) $1.8\,\mu$m, and (d) $2.0\,\mu$m.

$d_1/\Lambda = 0.55$. Interestingly, this curve is very flat and close to the zero-dispersion line, which is expected to be beneficial for improving SC generation efficiency. With larger Λ, the increase of d_1/Λ causes the dispersion curves to tend to move further away from the zero-dispersion line, shown in Figs. 2(b)–2(d). This means that the ZDWs are shifted towards the short wavelength, the fibers with smaller d_1/Λ are closer to the zero-dispersion line. In the case of small core PCFs, the competition between the matter dispersion and the waveguide dispersion could be the explanation for the diversity in dispersion characteristics. The material dispersion will exhibit influence for smaller d_1/Λ while the waveguide dispersion will have a stronger effect for larger d_1/Λ. It can be seen that modifying the structural parameters such as d_1 and Λ appropriately is an advantage for dispersion control.

The laser pump wavelength matches the wavelength at which the PCFs exhibit a normal or anomalous dispersion regime which determines the characteristics of the SC spectrum. The generation of SC light is done with a very broad spectrum even though the spectral time coherence is not high due to the intense laser pulses launched in an anomalous dispersion regime near ZDW. On the other hand, if the fiber is pumped in an all-normal dispersion regime, the SC spectrum spans with light pulses of high-time coherence and a preserved temporal profile. To diversify the applicability of generating SC suitable for the dispersion regime, we propose two PCFs with all-normal and anomalous flat dispersion, labeled as $\#F_1$ and $\#F_2$. $\#F_1$ fiber with $d_1/\Lambda = 0.55$ has the flattest dispersion among dispersion curves when lattice pitch $\Lambda = 1.0\,\mu$m and core diameter $D_c = 1.395\,\mu$m. This fiber has all-normal dispersion, and is expected to emit a broad and high coherence SC spectrum at a pump wavelength of $0.945\,\mu$m. $\#F_2$ has flat anomalous dispersion with $\Lambda = 2.0\,\mu$m, $d_1/\Lambda = 0.3$, with core diameter and $D_c = 3.34\,\mu$m larger than $\#F_1$ (Fig. 3(a)). The pump wavelength $1.4\,\mu$m corresponds to the normal dispersion region chosen close to ZDW ($1.414\,\mu$m). Thanks to the skillful adjustment of the diameter of the air holes in the innermost layer and the infiltration into the hollow core of PCF a liquid with high nonlinearity, the dispersion values at the pump wavelength of the two fibers $\#F_1$ and $\#\ F_2$ are -21.154 and -1.631 ps/nm.km, respectively, these values are smaller than some previous works.[29,32,33] The nonlinear coefficient of $\#F_1$ fiber is $486.355\,\mathrm{W}^{-1}\cdot\mathrm{km}^{-1}$, about nine times greater than that of $\#F_2$ fiber $50.669\ \mathrm{W}^{-1}\cdot\mathrm{km}^{-1}$ at pump wavelengths. Since the effective mode area is inversely proportional to the nonlinear coefficient (Eq. (4)), the effective mode area of $\#F_2$ fiber ($14.534\,\mu\mathrm{m}^2$) is larger than that of $\#F_1$ ($2.243\,\mu\mathrm{m}^2$) (Figs. 3(b) and 3(c)). Typically, smaller core PCFs will exhibit better light confinement in the core, i.e. higher nonlinear coefficients and smaller confinement losses. Our obtained effective mode area values are much smaller than some previous publications on $CHCl_3$ infiltrated PCF and other nonlinear liquids.[18,20,27,29,31,33] $\#\mathrm{F}_2$ fiber has higher confinement loss than $\#F_1$ (Fig. 3(d)). With a larger core, leakage of modes out of the core into the cladding and between the air holes could be the cause of this phenomenon. Although $\#F_2$ fiber has a higher confinement loss and lower nonlinear coefficient, the broad SC spectrum with soliton dynamics is still expected due to the flat dispersion and small

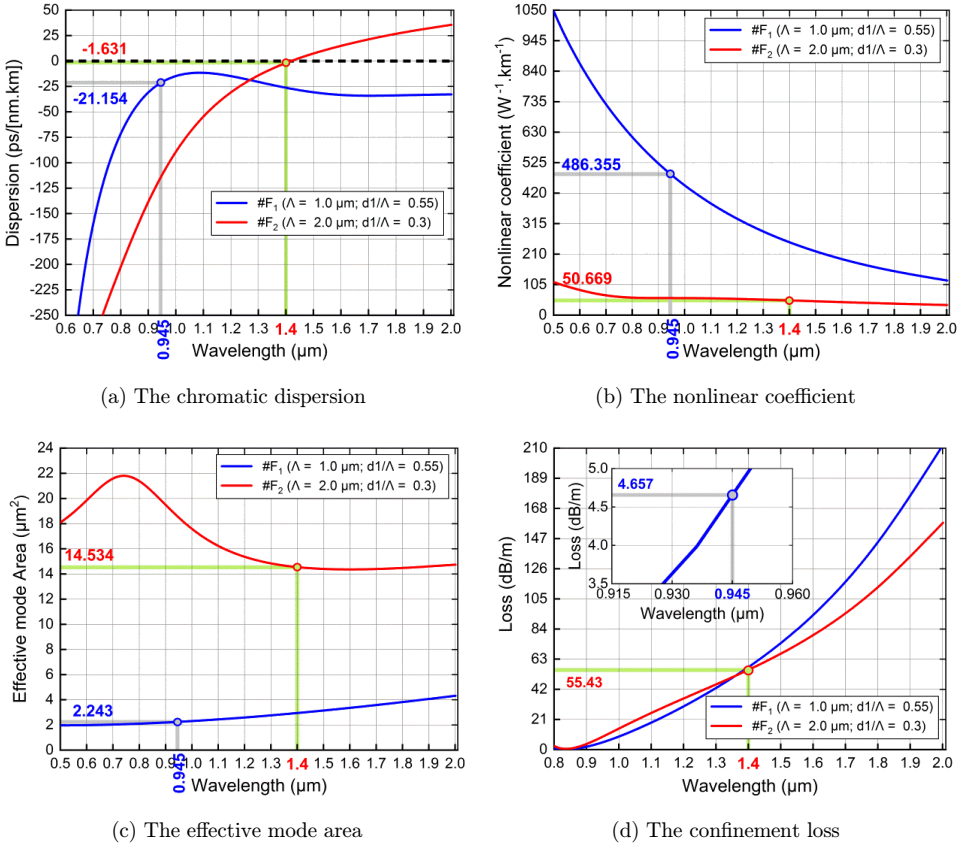

(a) The chromatic dispersion

(b) The nonlinear coefficient

(c) The effective mode area

(d) The confinement loss

Fig. 3. (Color online) The optical characteristics of the fundamental mode for $\#F_1$ and $\#F_2$ fibers.

Table 2. The structure parameters and the characteristic quantities of proposed PCFs at the pump wavelength in comparison with some previous work on liquid-filled PCFs.

#	D_c (μm)	Λ (μm)	d_1/Λ	Pump wavelength (μm)	A_{eff} (μm^2)	γ (W$^{-1}\cdot$km^{-1})	D (ps/nm$\cdot$km)	L_c (dB/m)
$\#F_1$	1.395	1.0	0.55	0.945	2.243	486.355	-21.154	4.657
$\#F_2$	3.34	2.0	0.3	1.4	14.534	50.669	-1.631	55.43

value at the pump wavelength. The structure parameters and the characteristic quantities of $\#F_1$ and $\#F_2$ at the pump wavelength are manifested in Table 2.

4. Supercontinuum Generation in Proposed Fiber

When dealing with very broad spectra, one sometimes has to take into consideration the high-order dispersion, even up to the sixth order. For light propagating in a waveguide such as PCF, the phase constant β is considered instead of the

wavenumber k. The propagation constant's expansion is calculated through the development coefficients of the Taylor series around the central angular frequency ω_0.[48]

$$\beta(\omega) = \beta(\omega_0) + \beta_1(\omega_0)(\omega - \omega_0) + \frac{1}{2!}\beta_2(\omega_0)(\omega - \omega_0)^2 + \cdot \tag{8}$$

The order dispersion term is related to the derivative of β with respect to the angular frequency ω, which is determined by the following equation:[50]

$$\beta_n = \left.\frac{d^n\beta}{d\omega^n}\right|_{\omega=\omega_0}. \tag{9}$$

Table 3 presents the higher-order dispersion at pump wavelength in our numerical model.

When the laser pulse propagates in a nonlinear medium, the spectrum is generated through the influence of dispersion and nonlinear processes. We numerically solve the generalized nonlinear Schrödinger equation (GNLSE), based on the split-step Fourier method.[48] The values of the higher-order dispersion are quite small, so the analysis results are only for the fundamental mode.

$$\partial_z\tilde{A} - i\tilde{\beta}(\omega)\tilde{A} - \frac{\tilde{\alpha}(\omega)}{2}\tilde{A} = i\gamma\left(1 + \frac{\omega - \omega_0}{\omega_0}\right)\tilde{A}F\left[\int_{-\infty}^{\infty} R(T')|A|^2(T - T')dT'\right], \tag{10}$$

where $\tilde{A}(z,\omega)$ is the Fourier transform of a pulse amplitude $A(z,T)$ and the nonlinear response function $R(T')$ is a sum of all contributing mechanisms listed by Zhao *et al.*[51] is the Raman response function. The left side of Eq. (9) depicts the linear propagation effects of the fiber, $\tilde{\alpha}$ and $\tilde{\beta}$ are attenuation and dispersion in the frequency domain, respectively. The right-hand side of Eq. (9) describes the nonlinear effects which depend on the nonlinear optical response of $CHCl_3$ determined by the combination of the bound-electronic and nuclear contribution. Nonlinear parameters are used in simulations.[51] The subscripts *el*, *d*, *l*, *c* indicate the following mechanisms: the bound-electronic, molecular reorientation, molecular interaction, and collision

Table 3. The coefficient of higher-order dispersion at the pump wavelength.

Coefficients	$\#F_1$	$\#F_2$
$\beta_2(\mathrm{ps}^2/\mathrm{m})$	1.01×10^{-2}	1.49×10^{-3}
$\beta_3(\mathrm{ps}^3/\mathrm{m})$	2.47×10^{-5}	1.11×10^{-4}
$\beta_4(\mathrm{ps}^4/\mathrm{m})$	9.31×10^{-8}	-1.73×10^{-7}
$\beta_5(\mathrm{ps}^5/\mathrm{m})$	7.7×10^{-10}	1.04×10^{-9}
$\beta_6(\mathrm{ps}^6/\mathrm{m})$	2.69×10^{-12}	-9.04×10^{-12}
$\beta_7(\mathrm{ps}^7/\mathrm{m})$	-2.95×10^{-13}	1.63×10^{-14}
$\beta_8(\mathrm{ps}^8/\mathrm{m})$	-6.11×10^{-16}	9.28×10^{-16}
$\beta_9(\mathrm{ps}^9/\mathrm{m})$	7.86×10^{-17}	-2.87×10^{-18}
$\beta_{10}(\mathrm{ps}^{10}/\mathrm{m})$	4.53×10^{-20}	-2.00×10^{-19}
$\beta_{11}(\mathrm{ps}^{11}/\mathrm{m})$	-1.88×10^{-20}	5.85×10^{-22}

induced, respectively, where $n_{2,el} = 0.41 \times 10^{-19}\,\mathrm{m^2W^{-1}}$, $n_{2,d} = 0.75\times 10^{-19}\,\mathrm{m^2W^{-1}}$, $\tau_{r,d} = 0.25\,\mathrm{ps}$, $\tau_{f,d} = 0.18\,\mathrm{ps}$, $n_{2,l} = 0.4 \times 10^{-19}\,\mathrm{m^2W^{-1}}$, $n_{2,c} = 0.08 \times 10^{-19}\,\mathrm{m^2W^{-1}}$, $\tau_{r,c} = 0.1\,\mathrm{ps}$, and $\tau_{f,c} = 0.1\,\mathrm{ps}$.

As the excitation pulse propagates along the $\#F_1$ and $\#F_2$ fiber lengths, the generated SC spectrum has significantly different characteristics depending on the behavior of the nonlinear effects. This is governed by the two proposed fibers' all-normal and anomalous dispersion properties. Despite having a larger dispersion value than $\#F_2$ fiber at the pump wavelength, with a much higher nonlinear coefficient and lower confinement loss, $\#F_1$ fiber has shown its advantage in SC spectrum generation with low power. The $\#F_2$ fiber, with a dispersion value as small as -1.631 ps/nm.km, generated a very broad SC spectrum despite the noise with higher peak power. SPM, followed by OWB, denotes the main nonlinear effects causing SC spectral broadening with the flat top because $\#F_1$ fiber has all-normal dispersion. Meanwhile, the appearance of solitons and dispersion effects will play a major role in broadening the SC spectrum for $\#F_2$ fibers with anomalous dispersion.

A narrow laser pulse with energy (E) varying from 0.01 nJ to 0.13 nJ and duration of 90 fs corresponding to peak power (P) 0.11–1.4 kW is injected into the $\#F_1$ fiber at wavelength of 0.945 μm, propagating for 10 cm in length, generating the SC spectrum with different widths is exposed in Fig. 4(a). When the input energy is as small as 0.01 nJ ($P = 0.11$ kW), the SC spectrum is still extended even though the width is negligible. Obviously, the spectral width increases as the input energy increases further. When the peak power reaches 0.78 kW (corresponding to 0.07 nJ pulse energy) the spectrum is quite broad and the top is flat. The maximum spectral width of 640.3 nm at relative intensity levels within 30 dB is achieved with a peak power of about 1.44 kW, corresponding to a pulse input energy of 0.13 nJ (Fig. 4(b)).

The temporal profile versus propagation length at various input pulse energies, and the pulse evolution of the SC along with fiber are indicated in Figs. 4(c) and 4(d). In the case of small peak power of 0.11 kW, only the SPM effect appears, making the SC spectrum broad and symmetric around the central wavelength. The symmetry of the SC spectrum will disappear with further increase of the peak power ($P \geq 0.194$ kW), the spectrum is broadened at the wings. SPM nonlinear effect followed by OWB and the influence of dispersion are the main reasons to explain this asymmetrical spectral broadening.[48,51] When the pulse with a peak power of 1.44 kW ($E = 0.13$ nJ) propagates in the $\#F_1$ fiber, the spectrum only broadens symmetrically at the first few centimeters of the propagation length due to the influence of SPM. As the pulse propagates further, the OWB appears due to a four-wave mixing effect, begins to show its impact at 2 cm of propagation length towards the blueshifted (trailing) edge of the pulse, and then that is 6 cm towards the redshifted (leading) edge of the pulse. As a result, new wavelength components are created and the SC spectrum is greatly expanded in both directions,[21] the group delay trace of the pulse is stretched out and the pulse spectrum becomes flatter on the wings (Fig. 4(c)). Unfortunately, the large dispersion and high dispersion slope at the short-wavelengths causes the spectrum not to broaden any further, spanning only to

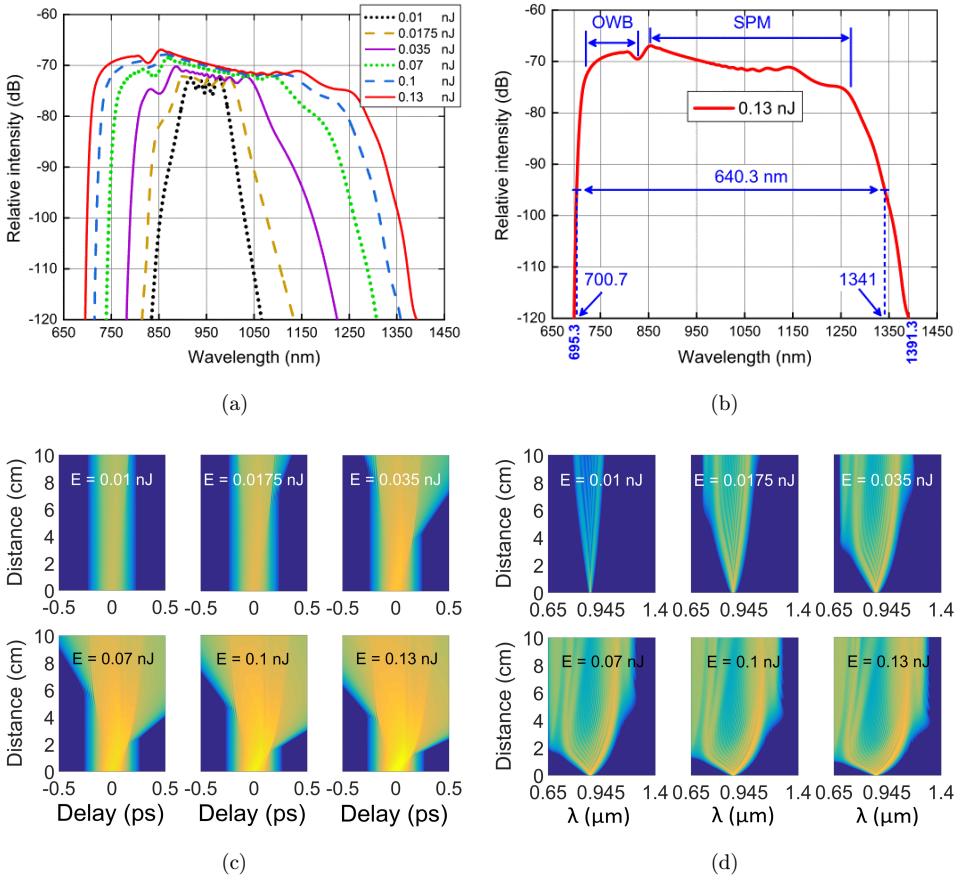

Fig. 4. (Color online) For $\#F_1$ fiber: (a) The output spectrum for various input pulse energies when using pump pulses with 0.945 μm pump wavelength and 90 fs duration, (b) the output spectrum with the input pulse energy of 0.13 nJ, (c) the temporal profile versus propagation length at various input pulse energies, and (d) the pulse evolution of the SC along with the fiber.

695.3 nm on the blue-side. On the red-side, the spectrum extends further to 1391.3 nm and is also limited by the low nonlinear coefficient.[25] We achieved a broad spectrum of 640.3 nm and flat-top with a low peak power of 1.44 kW. Even broader spectra can be obtained but the higher peak power and thermal evaporation of $CHCl_3$ must be taken into account.

In the following section, we will discuss how anomalous dispersion affects the SC spectrum expansion when $\#F_2$ fiber is pumped at 1.4 μm. The input pulse with energy of 0.01– 0.9 nJ with a duration of 45 fs (corresponding to a peak power of 0.22–20 kW) is pumped into the $\#F_2$ fiber with a length of 12 cm causing an extension of the output pulse, which is manifested in Figs. 5(a) and 5(b). The temporal profile versus propagation length at various input pulse energies and the pulse evolution of the SC along with fiber are denoted in Figs. 5(c) and 5(d). The spectrum

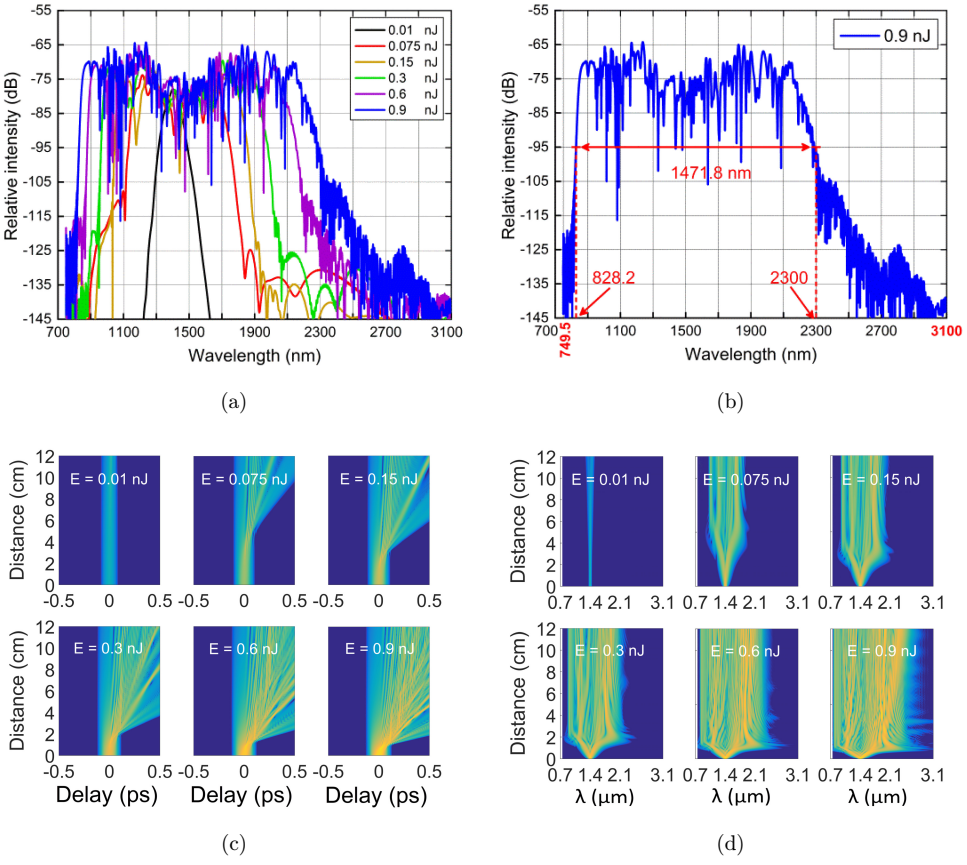

Fig. 5. (Color online) For $\#F_2$ fiber: (a) The output spectrum for various input pulse energies when using pump pulses with 1.4 μm pump wavelength and 45 fs duration, (b) the output spectrum with the input pulse energy of 0.9 nJ, (c) the temporal profile versus propagation length at various input pulse energies, and (d) the pulse evolution of the SC along with fiber.

is very broad, much more than $\#F_1$, and the noise peak is a fundamental feature of the spectrum when generating SC with anomalous dispersion PCF. The 1.4 μm pump wavelength of $\#F_2$ fiber is in the normal dispersion region but is very close to ZDW = 1.414 μm so the soliton dynamics, e.g., SF, SSFS, and DW[30] are the main mechanisms responsible for the spectrum expansion. However, the spectrum broadens significantly towards the red-side, which is attributed to the low-frequency shift of the soliton components due to the effect of the Raman SSFS effect.

The soliton does not appear when the input energy is not large enough. So the spectrum is very narrow and symmetric around the central wavelength thanks to the SPM when a narrow pulse of low peak power of 0.22 kW ($E = 0.01$ nJ) is injected into $\#F_2$ fiber (Figs. 5(a) and 5(c)). With $E = 0.075$ nJ ($P = 1.67$ kW), the soliton affects the spectral broadening and loses the symmetry of the spectrum as the input pulse moves at a longer propagation distance. As the peak power increases, the

spectral width increases markedly because the soliton dynamics give rise to new wavelength components. The maximum spectral width of 1471.8 nm within 30 dB (Fig. 5(b)) was obtained with a peak power of 20 kW ($E = 0.9$ nJ). Flat anomalous dispersion and small value -1.631 ps/nm $\cdot$ km at pump wavelength is one of the advantages of $\#F_2$ fiber, which positively affects spectral expansion despite the large effective mode area and high confinement loss.

In the case of input energy of 0.9 nJ, Figs. 5(c) and 5(d) show that the narrow pulse undergoes SPM which is compressed and symmetrically broadened only in the first few millimeters of the fiber length. Then, SF occurs at a propagation length of 1 cm as the input pulse approaches ZDW. Now, the first fundamental soliton with the shortest duration and highest energy among the fundamental solitons separated from the higher- order solitons and Raman scattering[30] undergoes SSFS shift towards the red-side due to stimulated Raman scattering.[52] This causes the spectrum to be shifted towards the red-side, extending to 3100 nm, and the longer wavelengths propagate more slowly in the anomalous dispersion region.[53] Meanwhile, the high dispersion slope in the short-wavelength region reduces the speed of the blue-shifted DWs as they catch up with the first ejected soliton. New wavelength components created through the FWM effect help the spectrum to be broadened to the blue-side up to 749.5 nm. In this case, we obtain a broad SC spectrum of 1471.8 nm corresponding to 30 dB range of relative intensity.

5. Conclusion

The high nonlinearity of $CHCl_3$ compared with silica and reasonable structural modification are important factors in optimizing dispersion and other nonlinear properties of optical fibers. That strongly affects the characteristics of the obtained SC spectrum. By infiltrating $CHCl_3$ into the hollow-core of the PCF in combination with the difference in air hole diameters in the structure, we have achieved flat all-normal and anomalous dispersion. Two proposed structures with small dispersion values at the pump wavelength, nonlinear coefficient, effective mode area, and confinement loss are suitable for SC generation. With the flat all-normal dispersion, nonlinear coefficients of 486.355 $W^{-1} \cdot km^{-1}$, and confinement losses as low as 4.657 dB/m, $\#F_1$ fiber with $\Lambda = 1.0\,\mu$m, $d_1/\Lambda = 0.55$ generates SC with a spectral width of 640.3 nm at a relative intensity of 30 dB when a laser pulse with a small peak power of 1.44 kW is excited at a central wavelength of 0.945 μm. As the pulse propagates within 10 cm of the fiber length, the SPM, followed by the OWB, denotes the nonlinear effects that govern the spectral expansion for this fiber. Soliton dynamics cause the SC spectrum to broaden when the laser pulse is injected into the $\#F_2$ fiber ($\Lambda = 2.0\,\mu$m, $d_1/\Lambda = 0.3$) at 1.4 μm. The flat anomalous dispersion, as small as -1.631 ps/nm.km, is also an important contributor to the spectral expansion of this fiber. We achieve a spectral width of up to 1471.8 nm within 30 levels dB when the pulse propagates at 12 cm of fiber length with a peak power of 20 kW.

Although $CHCl_3$ has a lower nonlinearity than other liquids such as C_2Cl_4, CS_2, C_7H_8, C_6H_6, $C_6H_5NO_2$, ... we have achieved a broader SC spectrum with lower peak power than in some previous works. We obtain a larger SC spectrum for $\#F_1$ fiber with all-normal dispersion than some publications.[20,27] Moreover, $\#F_2$ fiber with anomalous dispersion produces a much broader SC spectral than some works.[18,20,22,23,27,29,38] Even when compared with some previous publications on hollow core PCF filled with $CHCl_3$, our $\#F_2$ fiber still gives a much broader spectrum, the width is about 1.7 times that of Ref. 31, 1.4 times that of Ref. 32, and 1.85 times that of Ref. 33.

Acknowledgment

This research is funded by University of Education, Hue University under Grant Number NCM. T.23–02.

References

1. J. Pniewski, T. Stefaniuk, L. V. Hieu, C. L. Van, LanhC. V. R. Kasztelanic, G. Stepniewski, A. Ramaniuk, M. Trippenbach and R. Buczyński, *Appl. Opt.* **55**(19) (2016) 5033, doi: 10.1364/AO.55.005033.
2. T. S. Saini and R. K. Sinha, *Prog. Quantum Electron.* **78** (2021) 100342, doi: 10.1016/j.pquantelec.2021.100342.
3. H. Shang, D. Sun, M. Zhang, J. Song, Z. Yang, D. Liu, S. Zeng, L. Wan, B. Zhang, Z. Wang, Z. Li and Y. G. Liu, *J. Lightwave Technol.* **39**(12) (2021) 3890, doi: 10.1109/JLT.2020.3043022.
4. J. Zheng, J. Jiang, H. Chen, R. Zheng, X. Shen, K. Yu and W. Wei, *Opt. Laser Technol.* **138** (2021) 106832, doi: 10.1016/j.optlastec.2020.106832.
5. C. V. Lanh, N. T. Thuy, L. T. Bao Tran, H. T. Duc, V. T. M. Ngoc, V. L. Hieu and T. H. Van, *Photonics Nanostruct. Fundamentals Appl.* **48** (2022) 100986, doi: 10.1016/j.photonics.2021.100986.
6. M. Kalantari, A. Karimkhani and H. Saghaei, *Optik* **158** (2018) 142, doi: 10.1016/j.ijleo.2017.12.014.
7. L. Yang, B. Yan, R. Zhao, D. Wu, T. Xu, P. Yang, Q. Nie and S. Da, *Infrared Phys. Technol.* **113** (2021) 103576, doi: 10.1016/j.infrared.2020.103576.
8. C. V. Lanh, V. L. Hieu, D. N. Nguyen, V. T. M. Ngoc, H. D. Quang, T. H. Van, N. T. Thuy and C. V. Bien, *Laser Phys.* **32** (2022) 055102-12, doi: 10.1088/1555-6611/ac599b.
9. D. X. Khoa, C. V. Lanh, H. D. Quang, V. X. Luu, M. Trippenbach and R. Buczynski, *Appl. Opt.* **56**(4) (2017) 1012, doi: 10.1364/AO.56.001012.
10. D. X. Khoa, C. V. Lanh, C. L. Van, H. D. Quang, V. M. Luu, M. Trippenbach and R. Buczyński, *Opt. Quantum Electron.* **49**(2) (2017) 87, doi: 10.1007/s11082-017-0929-3.
11. M. Z. Alam, M. I. Tahmid, S. T. Mouna, M. A. Islam and M. S. Alam, *Opt. Commun.* **500** (2021) 127322, doi: 10.1016/j.optcom.2021.127322.
12. L. T. Bao Tran, N. T. Thuy, V. T. M. Ngoc, L. C. Trung, L. V. Minh, C. L. Van, D. X. Khoa and C. V. Lanh, *Photon. Lett. Poland* **12**(4) (2020) 106, doi: 10.4302/plp.v12i4.1054.
13. Y. Shen, A. A. Voronin, A. M. Zheltikov, S. P. O'Connor, V. V. Yakovlev, A. V. Sokolov and M. O. Scully, *Proc. SPIE 10522, Frontiers in Ultrafast Optics: Biomedical, Scientific, and Industrial Applications XVIII*, **10522**(2018) 105220I, doi: 10.1117/12.2285103.

14. M. Yamanaka, H. Kawagoe and N. Nishizawa, *Appl. Phys. Exp.* **9**(2) (2016) 022701, doi: 10.7567/APEX.9.022701.
15. Z. Dashtban, M. R. Salehi and E. Abiri, *Photon. Nanostruct. — Fundam. Appl.* **46**(2021) 100942, doi: 10.1016/j.photonics.2021.100942.
16. Y. J. You, C. Wang, Y. L. Lin, A. Zaytsev, P. Xue and C. L. Pan, *Laser Phys. Lett.* **13**(2) (2016) 025101, doi: 10.1088/1612-2011/13/2/025101.
17. A. Labruyère, A. Tonello, V. Couderc, G. Huss and P. Leproux, *Opt. Fiber Technol.* **18**(5) (2012) 375, doi: 10.1016/j.yofte.2012.08.003.
18. V. L. Hieu, T. H. Van, T. N. Hue, C. L. Van, R. Buczynski and R. Kasztelanic, *Opt. Quantum Electron.* **53** (2021) 187, doi: 10.1007/s11082-021-02820-3.
19. T. H. Van, R. Kasztelanic, G. Stepniewski, D. X. Khoa, C. L. Van, M. Trippenbach, M. Klimczak, R. Buczyński and J. Pniewski, *Appl. Opt.* **59**(12) (2020) 3720, doi: 10.1364/AO.385003.
20. Q. H. Dinh, J. Pniewski, H. L. Van, A. Ramaniuk, V. C. Long, K. Borzycki, K. D. Xuan, M. Klimczak and R. Buczyński, *Appl. Opt.* **57**(14) (2018) 3738, doi: 10.1364/AO.57.003738.
21. P. S. Maji and P. R. Chaudhuri, *Optik* **125**(20) (2014) 5986, doi: 10.1016/j.ijleo.2014.07.026.
22. V. L. Hieu, L. C. Van, T. N. Hue, M. N. An, R. Buczyński and R. Kasztelanic, *Laser Phys.* **28**(11) (2018) 115106, doi: 10.1088/1555-6611/aad93a.
23. N. T. Thuy, H. T. Duc, L. T. Bao Tran, D. V. Trong and C. V. Lanh, *J. Opt.* (2022), doi: 10.1007/s12596-021-00802-y.
24. C. V. Lanh, N. T. Thuy, H. T. Duc, L. T. Bao Tran, V. T. M. Ngoc, D. V. Trong, L. C. Trung, Q. H. Dinh and D. Q. Khoa, *Opt. Quantum Electron.* **54** (2022) 300, doi: 10.1007/s11082-022-03667-y.
25. C. V. Lanh, T. H. Van, C. L. Van, K. Borzycki, D. X. Khoa, T. Q. Vu, M. Trippenbach, R. Buczyński and J. Pniewski, *Opt. Eng.* **60**(11) (2021) 116109, doi: 10.1117/1.OE.60.11.116109.
26. S. Pricking and H. Giessen, *Opt. Exp.* **19**(4) (2011) 2895, doi: 10.1364/OE.19.002895.
27. C. V. Lanh, A. Anuszkiewicz, A. Ramaniuk, R. Kasztelanic, X. D. Khoa, M. Trippenbach and R. Buczynski, *J. Opt.* **19** (2017) 125604, doi: 10.1088/2040-8986/aa96bc.
28. M. Vieweg, T. Gissibl, S. Pricking, B. T. Kuhlmey, D. C. Wu, B. J. Eggleton and H. Giessen, *Opt. Exp.* **18**(24) (2010) 25232, doi: 10.1364/OE.18.025232.
29. C. V. Lanh, T. H. Van, C. L. Van, K. Borzycki, D. X. Khoa, T. Q. Vu, M. Trippenbach, R. Buczyński and J. Pniewski, *Laser Phys.* **30**(3) (2020) 035105, doi: 10.1088/1555-6611/ab6f09.
30. J. M. Dudley and J. R. Taylor, *Supercontinuum Generation in Optical Fibers* (Cambridge University Press, 2010), doi: 10.1017/CBO9780511750465.
31. H. Zhang, S. Chang, J. Yuan and D. Huang, *Optik* **121**(9) (2010) 783, doi: 10.1016/j.ijleo.2008.09.026.
32. C. C. Wang, W. M. Li, N. Li and W. Q. Wang, *Opt. Laser Technol.* **88** (2017) 215, doi: 10.1016/j.optlastec.2016.09.020.
33. V. L. Chu, V. T. Hoang, V. C. Long, K. Borzycki, K. D. Xuan, V. T. Quoc, M. Trippenbach, R. Buczyński and J. Pniewski, *Laser Phys.* **29**(7) (2019) 075107, doi: 10.1088/1555-6611/ab2115.
34. M. Chemnitz, C. Gaida, M. Gebhardt, F. Stutzki, J. Kobelke, A. Tünnermann, J. Limpert and M. A. Schmidt, *Opt. Exp.* **26**(3) (2018) 3221, doi: 10.1364/OE.26.003221.
35. T. Kato, Y. Suetsugu, M. Takagi, E. Sasaoka and M. Nishimura, *Opt. Lett.* **20**(9) (1995) 988, doi: 10.1364/OL.20.000988.

36. J. Challenor, *Toxicology of Solvents* (Rapra Technology Ltd, 2002), ISBN: 1-85957-296-0, doi: 10.1093/occmed/52.6.363-a.
37. M. Vieweg, S. Pricking, T. Gissibl, Y. Kartashov, L. Torner and H. Giessen, *Opt. Lett.* **37**(6) (2012) 1058, doi: 10.1364/OL.37.001058.
38. D. Churin, T. N. Nguyen, K. Kieu, R. A. Norwood and N. Peyghambarian, *Opt. Mater. Exp.* **3**(9) (2013) 1358, doi: 10.1364/ome.3.001358.
39. A. H. Bouk, A. Cucinotta, F. Poli and S. Selleri, *Opt. Exp.* **12**(5) (2004) 941, doi: 10.1364/OPEX.12.000941.
40. J. Liao and J. Sun, *Opt. Fiber Technol.* **18**(6) (2012) 457, doi: 10.1016/j.yofte.2012.07.006.
41. K. Saitoh, N. J. Florous and M. Koshiba, *Opt. Lett.* **31**(1) (2006) 26, doi: 10.1364/OL.31.000026.
42. C. Z. Tan, *J. Non-Cryst. Solids* **223**(1-2) (1998) 158, doi: 10.1016/s0022-3093(97)00438-9.
43. Z. Zhu and T. G. Brown, *Opt. Mater. Exp.* **10** (2002) 853, doi: 10.1364/OE.10.000853.
44. S. Kedenburg, M. Vieweg, T. Gissibl and H. Giessen, *Opt. Mater. Exp.* **2**(11) (2012) 1588, doi: 10.1364/OME.2.001588.
45. A. M. C. Davies, *NIR News*, 2005 — journals.sagepub.com, https://www.impopen.com/introduction-near-infrared-nir-spectroscopy.
46. I. Kubat and O. Bang, *Opt. Exp.* **24**(3) (2016) 2513, doi: 10.1364/OE.24.002513.
47. Y. S. Lee, C. G. Lee, F. Bahloul, S. Kim and K. Oh, *J. Lightwave Technol.* **37**(4) (2019) 1254, doi: 10.1109/JLT.2019.2891756.
48. G. P. Agrawal, *Nonlinear Fiber Optics*, 5th edn. (Academic Press, 2013), https://doi.org/10.1016/C2011-0-00045-5.
49. C. Wei, H. Zhang, H. L. Hongxi and S. Y. Liu, *Optik* **141** (2017) 32, doi: 10.1016/j.ijleo.2017.02.061.
50. R. Raei, M. E. Heidari and H. Saghaei, *J. Opt. Soc. Am. B* **35**(2) (2018) 323, doi: 10.1364/josab.35.000323.
51. P. Zhao, M. Reichert, S. Benis, D. J. Hagan and E. W. V. Stryland, *Optica* **5**(5) (2018) 583, doi: 10.1364/OPTICA.5.000583.
52. Y. Huang, H. Yang, S. Zhao, Y. Mao and S. Chen, *Res. Phys.* **23** (2021) 104033, doi: 10.1016/j.rinp.2021.104033.
53. S. Roy, D. Ghosh, S. K. Bhadra and G. P. Agrawal, *Opt. Commun.* **283**(15) (2010) 3081, doi: 10.1016/j.optcom.2010.04.003.